

Uncertainty Analysis for Spherical Near-Field Measurements*

Michael H. Francis and Ronald C. Wittmann †

Abstract— A general approach is introduced for estimating uncertainties in far-field parameters obtained from spherical near-field measurements. Although analysis is incomplete at present, we expect that as the measurement radius increases, our result will transform smoothly into the far-field case, where uncertainties depend on the on-axis gain and polarization of the probe and on the measurements in the far-field direction of interest.

Keywords: near-field measurements, spherical scanning, uncertainty

1. INTRODUCTION

UNCERTAINTY analysis for spherical near-field measurements is an on-going topic of research [1], [2], [3]. Previous work has relied heavily on simulation studies; however, we seek a more analytic approach patterned after [4] and [5].

Table 1 groups the uncertainty sources into twenty categories—four from the characterization of the probe and the remainder from the direct antenna under test (AUT) measurement. (This is a somewhat coarser division than proposed by Hess [6]). In this paper we restrict consideration to the underlying theory and some initial developments. We plan to report continuing progress in future presentations.

2. TRANSMISSION EQUATION

First, we note the far-field pattern of the AUT $\mathbf{t}(\hat{\mathbf{r}})$ in terms of the vector probe response \mathbf{w} is [8]

$$\mathbf{t}(\hat{\mathbf{r}}) = \sum (t_{nm}^1 \mathbf{X}_{nm}(\hat{\mathbf{r}}) + t_{nm}^2 \mathbf{Y}_{nm}(\hat{\mathbf{r}})), \quad (1)$$

where

$$\begin{pmatrix} t_{nm}^1 \\ t_{nm}^2 \end{pmatrix} = \mathbf{M}_n^{-1}(r) \begin{pmatrix} T_{nm}^1(r) \\ T_{nm}^2(r) \end{pmatrix} \quad (2)$$

*U.S. Government contribution not subject to copyright in the United States.

†National Institute of Standards and Technology, Boulder, CO 80305, francis@boulder.nist.gov

Inherited from Probe Measurement

1. Probe on-axis gain
2. Probe on-axis polarization
3. Relative probe pattern
4. Probe non- $\mu = \pm 1$ modes

Direct from AUT Measurement

5. Probe alignment
6. AUT alignment
7. Insertion loss
8. Impedance mismatch
9. Aliasing
10. Solid angle truncation
11. θ, ϕ position errors
12. r position errors
13. Probe-AUT multiple reflections
14. Non-linearity
15. I-Q imbalance
16. Flexing cables/ rotary joint errors
17. Drift
18. Leakage and crosstalk
19. Room scattering
20. Noise

Table 1. Sources of Uncertainty

and

$$T_{nm}^1(r) = \int \frac{\mathbf{w}(\mathbf{r})}{a_0} \cdot \mathbf{X}_{nm}^*(\hat{\mathbf{r}}) d\hat{\mathbf{r}} \quad (3)$$

$$T_{nm}^2(r) = \int \frac{\mathbf{w}(\mathbf{r})}{a_0} \cdot \mathbf{Y}_{nm}^*(\hat{\mathbf{r}}) d\hat{\mathbf{r}}.$$

Here, a_0 is proportional to the excitation amplitude and \mathbf{X}_{nm} and $\mathbf{Y}_{nm} = i\hat{\mathbf{r}} \times \mathbf{X}_{nm}$ are vector spherical harmonics [7, chpt. 16]. Further,

$$\mathbf{M}_n^{-1} = \frac{i\sqrt{(2n+1)/(4\pi)}}{2(R_{n,-1}^1 R_{n1}^2 - R_{n,-1}^2 R_{n1}^1)} \times \begin{pmatrix} -R_{n,-1}^2 - R_{n1}^2 & R_{n,-1}^2 + R_{n1}^2 \\ R_{n,-1}^1 + R_{n1}^1 & R_{n,-1}^1 - R_{n1}^1 \end{pmatrix}. \quad (4)$$

The $R_{n,\pm 1}^{1,2}$ are the translated probe coefficients and are known functions of the probe receiving pattern and the measurement radius r . It usually suffices to choose the mode limit so that

$$N \sim kr_{min}, \quad (5)$$

where r_{min} is the ‘‘minimum radius’’; that is, the radius of the smallest sphere, centered on the coordinate origin, that encloses the test antenna.

As r is increased

$$\mathbf{M}_n^{-1} \underset{r' \rightarrow \infty}{\sim} \frac{1}{2\pi\mathbf{s} \cdot \mathbf{s}} \begin{pmatrix} s_y & is_x \\ is_x & s_y \end{pmatrix} \frac{ikr}{\exp(ikr)}, \quad (6)$$

where

$$\begin{aligned} \mathbf{s} &= \mathbf{s}'_{\pi}(\hat{\mathbf{z}}) \\ s_x &= \mathbf{s}'_{\pi}(\hat{\mathbf{z}}) \cdot \hat{\mathbf{x}} \\ s_y &= \mathbf{s}'_{\pi}(\hat{\mathbf{z}}) \cdot \hat{\mathbf{y}} \end{aligned} \quad (7)$$

and $\mathbf{s}'_{\pi}(\hat{\mathbf{z}})$ is the receiving pattern on boresight when the probe is located at the origin of the laboratory coordinate system and is directed in the $-\hat{\mathbf{z}}$ direction.

3. UNCERTAINTY EQUATIONS

From (1) the uncertainty in the AUT far-field pattern becomes

$$\Delta \mathbf{t}(\hat{\mathbf{r}}) = \sum (\Delta t_{nm}^1 \mathbf{X}_{nm}(\hat{\mathbf{r}}) + \Delta t_{nm}^2 \mathbf{Y}_{nm}(\hat{\mathbf{r}})), \quad (8)$$

where

$$\begin{pmatrix} \Delta t_{nm}^1 \\ \Delta t_{nm}^2 \end{pmatrix} = \mathbf{M}_n^{-1} \begin{pmatrix} \Delta T_{nm}^1(r) \\ \Delta T_{nm}^2(r) \end{pmatrix} + \Delta \mathbf{M}_n^{-1} \begin{pmatrix} T_{nm}^1(r) \\ T_{nm}^2(r) \end{pmatrix} \quad (9)$$

and

$$\Delta T_{nm}^1(r) = \int \frac{\Delta \mathbf{w}(\mathbf{r})}{a_0} \cdot \mathbf{X}_{nm}^*(\hat{\mathbf{r}}) d\hat{\mathbf{r}} \quad (10)$$

$$\Delta T_{nm}^2(r) = \int \frac{\Delta \mathbf{w}(\mathbf{r})}{a_0} \cdot \mathbf{Y}_{nm}^*(\hat{\mathbf{r}}) d\hat{\mathbf{r}}.$$

The uncertainty due to the probe is (from 4)

$$\begin{aligned} \Delta \mathbf{M}_n^{-1} &= \frac{i\sqrt{(2n+1)/(4\pi)}}{2(R_{n,-1}^1 R_{n1}^2 - R_{n,-1}^2 R_{n1}^1)} \\ &\times \Delta \begin{pmatrix} -R_{n,-1}^2 - R_{n1}^2 & R_{n,-1}^2 + R_{n1}^2 \\ R_{n,-1}^1 + R_{n1}^1 & R_{n,-1}^1 - R_{n1}^1 \end{pmatrix} \quad (11) \\ &+ \mathbf{M}_n^{-1} \Delta \left(\frac{1}{R_{n,-1}^1 R_{n1}^2 - R_{n,-1}^2 R_{n1}^1} \right), \end{aligned}$$

where

$$\begin{aligned} \Delta R_{nm}^1(r) &= \int \Delta \mathbf{s}'_{\pi}(\hat{\mathbf{k}}) \cdot \mathbf{X}_{nm}(\hat{\mathbf{k}}) e^{i\gamma r} \frac{d\mathbf{K}}{\gamma k} \\ \Delta R_{nm}^2(r) &= \int \Delta \mathbf{s}'_{\pi}(\hat{\mathbf{k}}) \cdot \mathbf{Y}_{nm}(\hat{\mathbf{k}}) e^{i\gamma r} \frac{d\mathbf{K}}{\gamma k}. \end{aligned} \quad (12)$$

Here, we are restricted to a symmetric $m = \pm 1$ probe, as usually employed in spherical near-field scanning.

The first term in (9) is due to the uncertainty in the measured near field and the second term is due to the uncertainty in the properties of the probe. (This corresponds to the division of Table 1.) A similar separation arises in the planar near-field case [4, eq. (26)].

4. UNCERTAINTY ANALYSIS

Our intent is to estimate uncertainties in the measured AUT data and the probe pattern, and to propagate them through the above equations to the far field (8). We will use a worst-case analysis (particularly when errors are small) or a statistical (RMS) approach where applicable. Many details are unclear at this time.

When the measurement radius is large, the far-field pattern is given by

$$\mathbf{t}(\hat{\mathbf{r}}) \underset{r \rightarrow \infty}{\sim} \frac{1}{2\pi\mathbf{s} \cdot \mathbf{s}} \frac{ikr}{\exp(ikr)} \left[s_y \frac{\mathbf{w}(\mathbf{r})}{a_0} + s_x \frac{\mathbf{w}(\mathbf{r}) \times \hat{\mathbf{r}}}{a_0} \right], \quad (13)$$

where we have used (6). It is easy to show that if s_x/s_y is essentially real (corresponding to a linearly polarized probe), the uncertainty approaches the simple form

$$\frac{\|\Delta\mathbf{t}(\hat{\mathbf{r}})\|^2}{\|\mathbf{t}(\hat{\mathbf{r}})\|^2} \underset{r \rightarrow \infty}{\sim} \frac{\|\Delta\mathbf{s}\|^2}{\|\mathbf{s}\|^2} + \frac{\|\Delta\mathbf{w}(\mathbf{r})\|^2}{\|\mathbf{w}(\mathbf{r})\|^2}. \quad (14)$$

In this case, the overall uncertainty depends only on uncertainties in the on-axis properties of the probe and uncertainties in the measured field in the direction of interest.

As the measurement radius decreases into the near-field region, more of the measured near field influences the far-field result in a given direction. Following Yaghjian [9], we expect most of the uncertainty contributions to come from the probe pattern and measured near field over the mutually subtended solid angle illustrated in Figure 1.

5. CONCLUSION

We have laid a foundation for future development of an uncertainty analysis for spherical near-field scanning measurements. This analysis divides neatly into terms due to uncertainties in the probe properties and to uncertainties in the near-field measurements. We expect the spherical near-field uncertainty analysis to approach the well-known far-field uncertainty analysis as the measurement radius increases.

REFERENCES

[1] Hansen, J. E., *Spherical Near-field Antenna Measurements*, Chap. 6, Peter Peregrinus Ltd., 1988.

[2] Newell, A.C.; Hindman, G. and Stubenrauch, C.F., "The Effect of Measurement Geometry on Alignment Errors in Spherical Near-Field Measurements," *Proc. Ant. Meas. Tech. Assoc.*, pp. 274–279, October 1999.

[3] Newell, A.C. and Hindman, G., "The Alignment of a Spherical Near-Field Rotator Using Electrical Measurements," *Proc. Ant. Meas. Tech. Assoc.*, pp. 131–136, October 1997.

[4] Newell, A.C., "Error Analysis Techniques for Planar Near-Field Measurements," *IEEE Trans. Antennas Propagat.*, vol. AP-36, no. 6, pp. 754–768, June 1988.

[5] Newell, A.C. and Lee, D. "Application of the NIST 18 Term Error Model to Cylindrical Near-Field Antenna Measurements," *Proc. Ant. Meas. Tech. Assoc.*, pp. 24–29, October 2000.

[6] Hess, D.W., "An Expanded Approach to Spherical Near-Field Uncertainty Analysis," *Proc. Ant. Meas. Tech. Assoc.*, pp. 495–500, October 2002.

[7] Jackson, J. D., *Classical Electrodynamics*, 2nd ed.

[8] Wittmann, R. C. and Francis, M. H., "Spherical Near-Field Scanning Algorithms," To be published.

[9] Yaghjian, A. D.: "Efficient Computation of Antenna Coupling and Fields Within the Near-Field Region," *IEEE Trans. Antennas Propagat.*, vol. AP-30, pp. 113–128, January 1982.

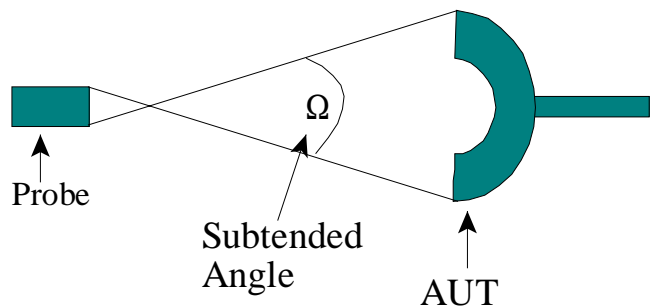


Figure 1 – Schematic showing the subtended angle between the probe and AUT.